Mohammad Y. Hajeer, DDS
PhD student in Orthodontics

Ashraf F. Ayoub, FDSRCPS, MDS, FDSRCS, PhD
Senior Lecturer/Honorary Consultant in Oral and Maxillofacial Surgery
Leader of Biotechnology and Craniofacial Research Group

Declan T. Millett, BDSc, FDS, DDS, DOrth, MOrth
Senior Lecturer/Honorary Consultant in Orthodontics

University of Glasgow Dental School
Glasgow, United Kingdom

Mitchum Bock, BSc, BMath, PhD
Lecturer
Department of Statistics

J. Paul Siebert, BSc, PhD, MIEE, CEng
Senior Research Fellow
Department of Computing Science

University of Glasgow
Glasgow, United Kingdom

Reprint requests:
Dr A. F. Ayoub
Department of Oral and Maxillofacial Surgery
Glasgow Dental Hospital and School
378 Sauchiehall Street
Glasgow G2 3JZ
United Kingdom
Fax: +44-141-2119601
E-mail: a.ayoub@dental.gla.ac.uk

Int J Adult Orthod Orthognath Surg
Vol. 17, No. 4, 2002

Three-dimensional imaging in orthognathic surgery: The clinical application of a new method

Many 3-dimensional (3D) techniques have been utilized to register and analyze the face in 3 dimensions, but each system has its own merits and disadvantages. C3D is a relatively new 3D imaging system that was developed to capture the 3D geometry of the face. Landmark identification on 3D facial models is facilitated by a software-based facial analysis tool developed by the authors. The reproducibility of landmark identification was high for 20 of the chosen points (standard deviations of repeated placements of landmarks around their centroids were 0.5 mm or less). The method is useful in studying facial soft tissue changes following orthognathic surgery and other types of facial surgery, as well as assessing facial soft tissue growth and development of the craniofacial complex. (Int J Adult Orthod Orthognath Surg 2002;17:318–330)

The correction of dentofacial deformities requires teeth and jaws to be manipulated in 3 dimensions to achieve the best results within the constraints of esthetics, stability, and function. Assessment of facial appearance, although clearly a 3-dimensional (3D) problem, has been attempted with 2D photographs and radiographs.[1]

Many 3D techniques have been used in attempts to capture facial topography and to meet the shortcomings of conventional 2D (photograph or radiograph) methods. These techniques have included: morphanalysis,[2] laser scanning,[3,4] 3D computerized tomographic (CT) scanning,[5] stereolithography,[6] 3D ultrasonography,[7] 3D facial morphometry,[8,9] digigraph imaging,[10] Moiré topography,[11] and contour photography.[12]

This paper aims to review the techniques that have been employed to capture 3D data of patients' faces, discussing their advantages and their possible shortcomings. The application of a new stereophotogrammetric technique is presented, and the reproducibility of identifying landmarks is evaluated.

Review of techniques

3D cephalometry

3D cephalometry is based on manual techniques for abstracting 3D coordinate data from 2 biorthogonal head films, ie, lateral and anteroposterior radiographs.[13–15] The main drawbacks of this technique are patient exposure to radiation, difficulties in locating accurately the same landmarks in 2 biorthogonal radiographs, lack of soft tissue contour assessment, and the time-consuming nature of the procedure.

Morphanalysis

Morphanalysis is a method of obtaining 3D records using photographs, radiographs, and study casts of a patient. Rabey[2] claimed that the principal benefits of morphanalysis in orthognathic surgery were analytic validity, statistical validity, accuracy, and superior communications. The equipment, however, is extremely elaborate and expensive. The technique is time consuming and not very practical for everyday use.

CT-assisted 3D imaging

In the mid-1980s, CT-assisted 3D imaging and modeling of the skull structures were introduced for use in maxillofacial surgery.[5] The main disadvantages of this technique are: *(1)* patient exposure to a high radiation dose (therefore, it is not suitable for long-term assessment following orthognathic surgery); *(2)* limited resolution of facial soft tissues due to slice spacing, which can be 5 mm or more; and *(3)* presence of artifacts created by metal objects such as dental restorations and fixed orthodontic appliances, because of the reduced penetrability.

Recently, Xia et al[16,17] developed a system for reconstructing 3D soft and hard tissues from sequential CT slices using a surface rendering technique followed by extraction of facial features from 3D soft tissues. A conformed facial mesh was constructed from a generic mesh. Three digitized color portraits were texture-mapped onto the 3D head mesh. Although this technique was interesting in showing the importance of having the full-color details of patients' faces in the final output, the validity of the construction process was not evaluated. The three 2D color portraits were taken on a different occasion from CT scanning, with potential changes in facial expression. Also, the accuracy of the reconstructed 3D soft tissue model is affected by the long capture time (approximately 2 seconds), which would not be suitable for use in children. In addition, tests for reproducibility of landmark identification were not performed to assess the accuracy of facial texture mapping.

Stereolithography

Stereolithography is a method of organic model production based on CT scans that enables the representation of complex 3D anatomic structures.[6] The obvious shortcomings of this technique are: *(1)* the need for experienced and skilled operators to obtain accurate 3D modeling; *(2)* expense of the method; *(3)* patient exposure to radiation for CT scans; and *(4)* no production of soft tissue in machine-readable form.[1]

3D laser scanning

Laser scanning techniques provide a less invasive method for capturing the maxillofacial region in 3 dimensions. They have been used in clinical auditing of surgical outcome and measurement of surgical relapse.[3,4] The data are stored in computer memory and approximately 20,000 coordinates on the facial surface are derived. The shortcomings of this technique are: *(1)* slowness of method, which takes 8 to 10 seconds to scan the face, making distortion of the scanned image likely; *(2)* need for the patient's eyes to be closed during scanning, for protection, which may bring into question the identity of the captured image; and *(3)* inability to capture the soft tissue surface texture, which results in difficulties in identification of landmarks that are dependent on surface color. While white-light laser approaches (eg, supplied by ARIUS3D) are now capable of imaging surface texture color, the shortcomings listed above persist.

Moiré topography and contour photography

Both Moiré topography and contour photography use grid projections during exposure, resulting in standardized contour lines on the face.[11,12] Moiré topography delivers 3D information based on the contour fringes and fringe intervals. Difficulties are encountered if a surface has sharp features, so these 2 methods are suitable to use on smoothly contoured faces. However, great care is needed in positioning the head, as a small change in head position produces a large change in fringe pattern. A 3D measuring system was proposed by Motoyoshi et al,[18] but this system does not capture the normal facial texture, and subsequent landmark identification is difficult. The authors did not propose any objective method for studying facial changes following surgery.

3D facial morphometry

This system comprises 2 charge-coupled device (CCD) cameras that capture the subject, real-time hardware for the recognition of markers placed on patients'

faces, and software for the 3D reconstruction of landmarks' x,y,z coordinates relative to a reference system.[8,9,19] The process of placing landmarks on the face is time- and labor-consuming and cannot be performed consistently between consecutive sessions due to movement of facial features. Although the system has been used extensively to investigate facial changes, no lifelike models have been produced to show the natural soft tissue appearance of faces. This system could not be used as a 3D treatment-planning tool or as a communication medium with orthognathic surgery patients.

3D ultrasonography

Ultrasonography was introduced recently to capture 3D data. This technique delivers a reflection picture, which is transformed into digital information.[7] Ultrasonography waves do not visualize bone or pass through air, which acts as an absolute barrier during both emission and reflection. Therefore, a specific contact probe is required to generate a 3D database. This system gives the 3D coordinates of the landmarks chosen, but it will not produce a 3D image. The procedure is time consuming and necessitates a cooperative patient as well as a skillful operator. Motion of the head during data acquisition introduces errors, while touching facial soft tissues may cause distortions of their spatial positions.

Stereophotogrammetry

Early stereophotogrammetry. Photogrammetry is defined as "the science or art of obtaining reliable measurements by means of photographs."[20] Stereophotogrammetry refers to the special case where 2 cameras, configured as a stereopair, are used to recover the 3D distance to features on the surface of the face by means of triangulation. This technique has evolved to provide a more accurate evaluation of the face and may adopt 1 or more stereo-pair views to increase the number of 3D measurements that can be obtained to compute a 3D facial surface model. To reduce inaccuracy due to movement, photographs from each side of the face are taken simultaneously; also, the duration of exposure has been reduced with improvement in technology.

Clinical use of stereophotogrammetry was first reported by Thalmann-Degan in 1944 according to Burke and Beard.[21] Several stereophotogrammetric techniques were proposed in the literature before the creation of contemporary digital stereophotogrammetry.[21–25]

Contemporary digital stereophotogrammetry. The incorporation of recent technology has given the ability to process complex algorithms to convert simple photographs to 3D measurements of facial changes. Kobayashi et al[26] used reference points marked on the face, a metal reference frame, a pair of cameras, and a computer to produce 3D wireframe models that could be viewed from any angle. The soft tissue analysis consisted of calculating 3D values of reference points on the face by perspective transformation of their values into 2 pairs of photographs.[26] Ras et al[27] demonstrated a stereophotogrammetric system that gives the 3D coordinates of any chosen facial landmark. However, the configuration of their system did not cover the whole face, and the final output lacked the color information needed for accurate landmark identification.

Techalertpaisarn and Kuroda[28] used 2 LCD projectors, CCD cameras, and a computer to produce a 3D image of the face that could be edited, shifted, or rotated in any direction. This system needed at least 2 seconds to capture an image through 8 projecting alternating patterns of black and white stripes (structured light) onto the patient's face. This is too long to be reliable in avoiding head movements, especially in children. Also, no lifelike soft tissue models are produced by this method.

Recently, Nguyen et al[29] described a 3D imaging system that required structured light to capture patients' faces. With this system, however, there is a high possibility of having jagged areas on the reconstructed image because of head movements between multiple captures.

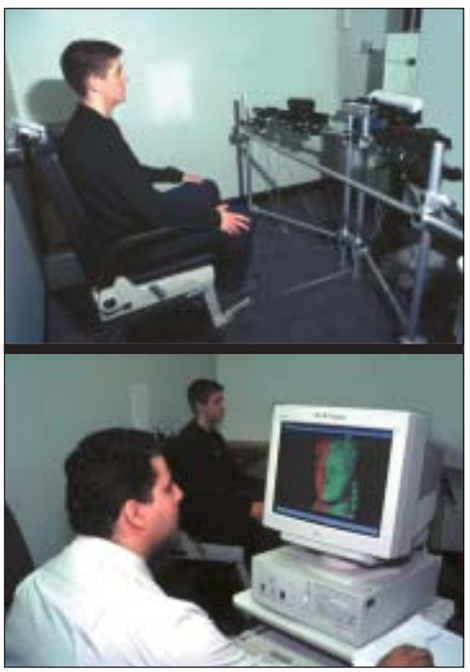

Fig 1 *(left)* To begin the process, the patient sits on a chair in front of the system with the head in natural head position. Six images are captured within 50 milliseconds and transferred to the computer, where the operator can check the quality of the image before constructing 3D models.

Fig 2 *(below)* The components of a capture pod: 1 color camera, 2 monochrome cameras, 1 white-light flash, and 1 speckle texture projection flash.

C3D: A 3D non-contact vision-based imaging system

C3D was based on the Active Stereo Probe,[30–32] funded by the UK Department of Trade and Industry, which employed a new image-matching algorithm.[32] The C3D system was developed for clinical applications[33] in a collaboration between Glasgow University Dental School and the Turing Institute and then subsequently with the Department of Computing Science at Glasgow University. Currently, C3D range imaging is based on the use of stereo-pairs of digital cameras and special textured illumination,[34] which provides quick capture times (30 milliseconds) and makes the system appropriate for imaging children and infants, as well as adults (Fig 1). The longer the exposure (or data capture time), the more unreliable or blurred the imaged data becomes; this has important implications if measurement of the face to submillimeter accuracy is required. A third digital camera (full color) is appended to each stereo-pair to enable C3D to capture the natural surface appearance of the patient's skin and then "drape" this skin texture over the constructed 3D model of the face (Figs 2 to 4). Accordingly, C3D provides the clinician with a lifelike 3D model of the patient's head that can be rotated, enlarged, and measured in 3 dimensions as required for diagnosis, treatment planning, and surgical outcome analysis. A fuller account of the C3D imaging process is presented elsewhere.[34] The accuracy of the system was evaluated by Ayoub et al[35] by comparing x,y,z coordinates of specific landmarks digitized from on-screen 3D models for 21 plaster casts of cleft models, with the x,y,z coordinates derived directly from these models using a previously validated 3D contact ultrasonic measuring system at the School of Manufacturing and Mechanical Engineering, University of Birmingham. The overall error between both measurements was below 0.6 mm, which was acceptable for studying facial soft tissue changes.[35]

How C3D system works. C3D configured for clinical facial imaging consists of 2 pods, and each pod consists of 3 cameras (Fig 2). Two monochrome cameras serve to form a stereo baseline and are synchronized to capture images illuminated by special texture flash projectors (Fig 3a). A third central color camera is synchronized to capture the natural photographic appearance of the subject under normal white-light flash, just 20 milliseconds after

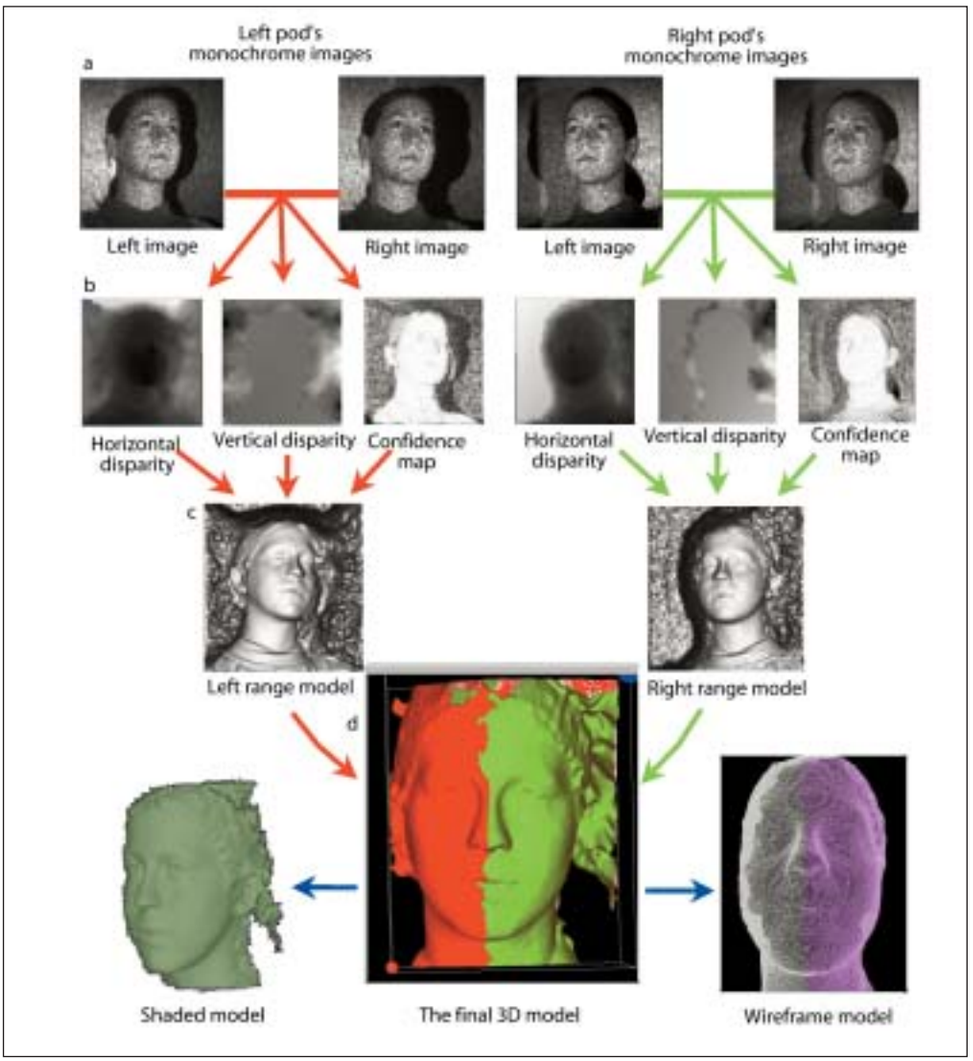

Fig 3 **(a)** Two-dimensional raw data are captured from each pod. Each pod produces 1 color image illuminated with white-flash and 2 black-and-white images illuminated with texture projection. **(b)** XY disparities and confidence maps are constructed through stereo-pair matching. **(c)** Range models are recovered from each stereo-pair. **(d)** A 3D model is constructed that can be viewed as a shaded model or as a wireframe model.

the flash texture stereo-capture (Fig 4). So that the detailed geometric configuration of all of the cameras can be determined, a calibration target (comprising discs on contrasting background and of accurately known dimensions and location) is presented and captured by the cameras for a variety of target poses (Fig 5).

The complex nature of the process is to determine, for each point imaged in the left camera, the corresponding point in the right camera. The output of this process is (x,y) disparity maps and a confidence map (Fig 3b). The point cloud captured by a single stereo-pair of cameras comprises only 2.5D information and is called a *range model* (Fig 3c). This point cloud can be warped easily to fit a triangulated mesh.[34] An implicit surface is computed that merges together the point clouds into a single triangulated polygon mesh, using a variant of the Marching Cubes algorithm.[36] This mesh is then further decimated to any arbitrarily low resolution for display purposes. The final 3D output can be seen as a solid (green and red), shaded, or wireframe

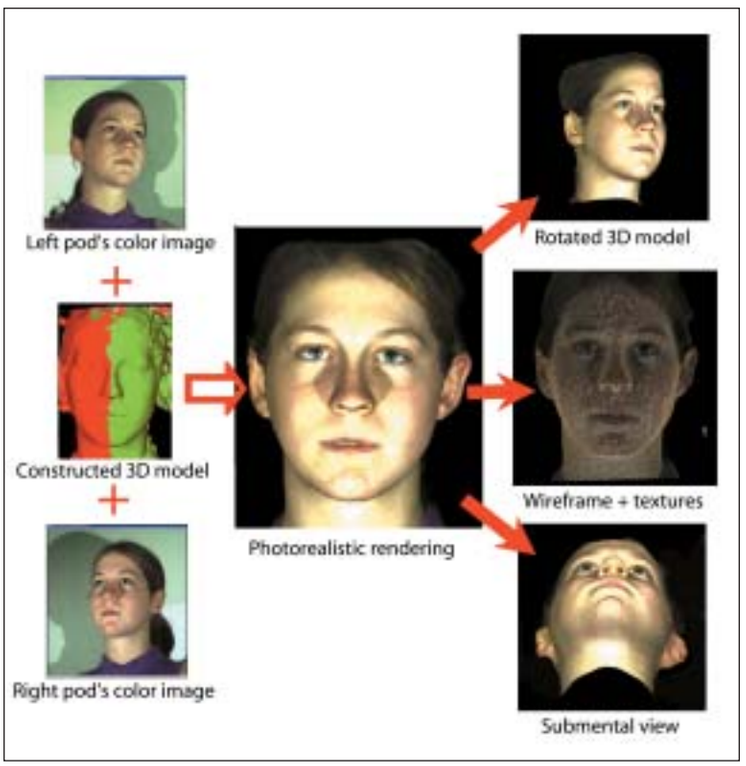

Fig 4 Facial texture mapping. The 2 color images are merged and mapped onto the constructed 3D model in the photorealistic rendering. The final model can be viewed from any direction.

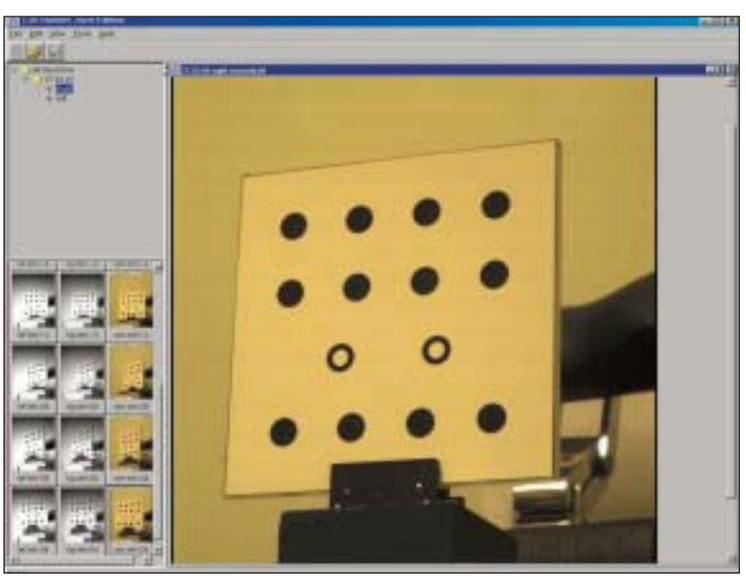

Fig 5 Calibration target. The calibration target is imaged several times in different positions. Images taken from the 6 cameras are processed to find the central location of the discs and used to fit a geometric model of each camera and its respective orientation to the target.

model (Fig 3d). By finding the correspondence between each vertex in the 3D polygonal mesh and each pixel in the color texture map, the system creates a photorealistic rendered model that can be viewed from any direction (Fig 4).

Landmark identification on 3D facial models: Facial analysis tool. Landmark identification is the first step toward building the origins of a coordinate system, constructing additional pseudo-landmarks, creating curved data or specific contours, enclosing surface areas by boundary landmarks, enabling volumetric measurements, and evaluating shape change using different analyses. To abstract soft tissue

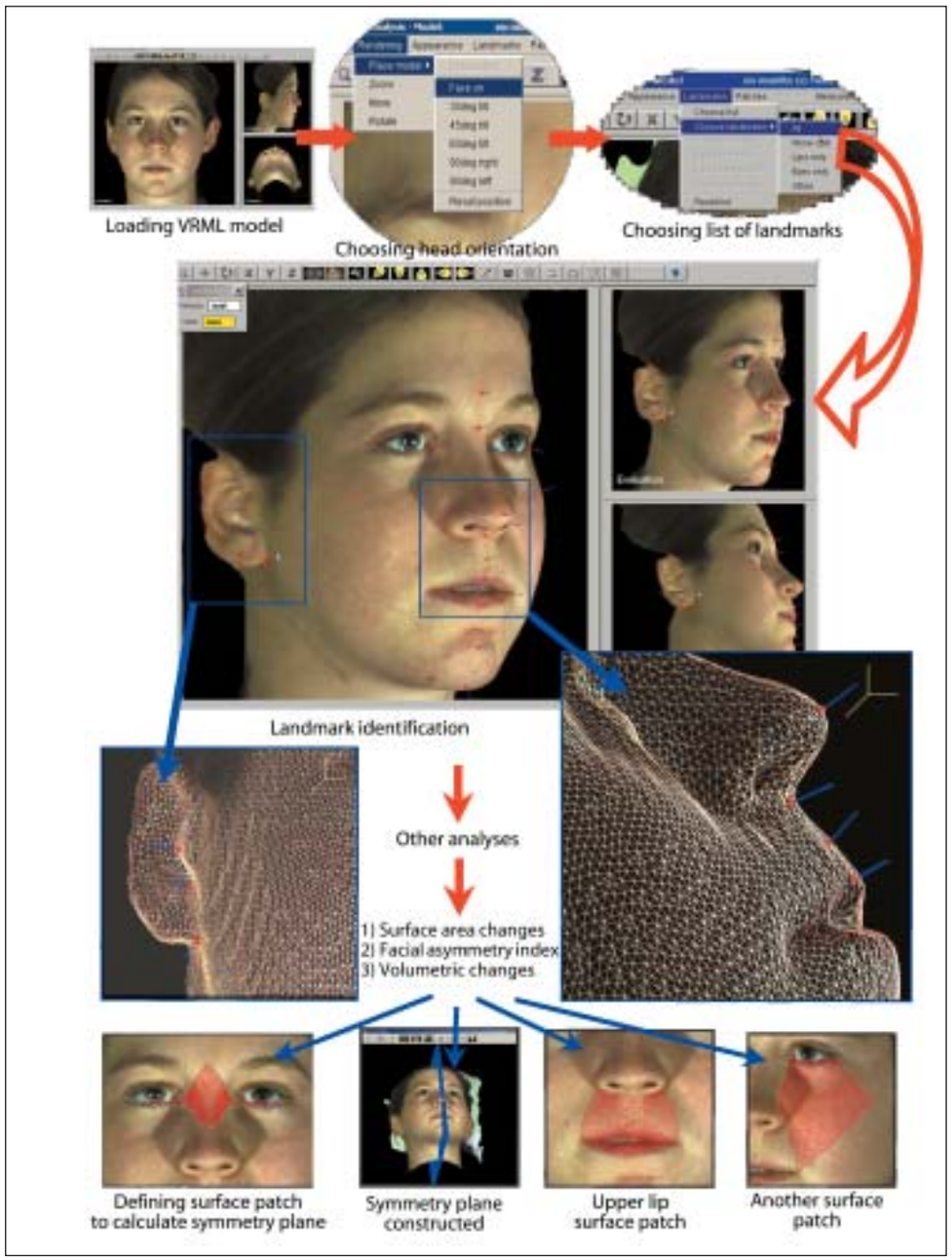

Fig 6 The interface of the facial analysis tool. After loading the 3D model, the orientation of the face is defined, and a list of landmarks is chosen. Landmark identification is carried out using 3 different windows, where the model can be manipulated independently. The operator can define surface patches to calculate a symmetry plane and to measure surface area and volumetric changes.

landmarks from C3D facial models of patients undergoing orthognathic surgery, a software-based facial analysis tool (FAT)[37] was developed within a collaborative project to assess facial clefts in babies and infants. Each model is loaded to the FAT, where the operator can manipulate the model from any point of view through the use of magnification, translation, and rotation buttons (Fig 6). The operator has a choice of 6 different predefined positions to standardize the orientation of the head.

When the procedure of landmark identification is complete, the software generates a text file containing x,y,z coordinates of the chosen landmarks. This 3D set of data can

Fig 7 Three-dimensional meshes of a skeletal Class III case *(left)* preoperatively and *(right)* postoperatively.

be manipulated using one of the available statistical shape analyses, eg, generalized Procrustes analysis or principal component analysis. The FAT provides the operator with other functionalities, such as identifying boundary landmarks to create patches on the model, which can help in measurement of surface area and volumetric changes and assessment of facial asymmetry (Fig 6).

Reproducibility of landmark identification: The experiment

Subjects and methods

Ten 3D models were chosen randomly from our database of orthognathic surgery cases (5 presurgical and 5 postsurgical). An example of a 3D model of a Class III case captured before and after surgery is shown in Fig 7. Thirty landmarks were identified on-screen for each model by one operator (MYH). Twelve landmarks were identified in the midsagittal plane, and 9 were bilateral ones. Most of these landmarks were defined according to Farkas[38] (Table 1). The procedure of landmark identification was repeated 3 times, with a 1-week gap between each session of digitization. The FAT was used to obtain the x,y,z coordinates of the identified landmarks. Differences in x-, y-, and z-axes for each landmark were calculated, and the mean differences from the 3 comparisons (T1-T2, T2-T3, and T1-T3) were obtained. In addition, standard deviations (SD) of landmarks around their centroids were obtained for the 30 landmarks.

Results

Table 2 illustrates the amount of error in landmark identification for each landmark in the x-, y-, and z-axes. If we consider 0.5 mm as a cutoff limit between reproducible and non-reproducible landmarks, 5 landmarks were above this limit in the x- (transverse) direction (left and right Go, left and right Zyg, and Me), while 25 landmarks showed high reproducibility (< 0.5 mm). The most reproducible landmarks were left and right Sbtr, Ac, and Sn. In the y-axis (vertical), irreproducibility was limited to the previously mentioned bilateral points of Go and Zyg as well as Gl, and left and right Tr. However, Me showed an acceptable amount of reproducibility (0.4 mm). The number of irreproducible landmarks increased to 8 when we looked at the mean differences in the z-axis (anteroposterior). Again, left and right Go were the most irreproducible landmarks, followed by left and right Tr, Me, and left and right Obi. Most of the midsagittal landmarks were highly reproducible in the anteroposterior direction, with a landmark identification error varying from 0.05 mm (for SLs) to 0.23 mm (for Sn).

The overall reproducibility of each landmark is shown in Fig 8, where standard deviations (SD) of landmarks' coordinates around their centroids were obtained (combining the x-, y-, and z-axes differences together). If we consider any landmark with a standard deviation at or below 0.5 mm as a highly reproducible point, 20 landmarks were found to fit in this category. However,

Table 1 Landmark definitions according to Farkas[38]

Landmark	Definition
Alar curvature (or alar crest) (Ac)	The most lateral point in the curved base line of each ala, indicating the facial insertion of the nasal wingbase
Cheilion (Ch)	The point located at each labial commissure
Endocanthion (Enc)	The point at the inner commissure of the eye fissure, located lateral to the bony landmark used in cephalometry
Exocanthion (Exc)	The point at the outer commissure of the eye fissure, located slightly medial to bony exocanthion
Glabella (Gl)	The most prominent midline point between the eyebrows, identical to bony glabella on the frontal bone
Gonion (Go)	The most lateral point on the mandibular angle close to bony gonion
Inferior labial sulcus (ILs) (sublabiale*)	The deepest midline point on the labiomental fold, which determines the lower border of the lower lip or the upper border of the chin
Labrale inferius (Li)	The midpoint of the lower vermilion line
Labrale superius (Ls)	The midpoint of the upper vermilion line
Menton (Me)	The lowest median landmark on the lower border of the mandible, identical to bony menton
Nasion (N)	The point in the midline of both the nasal root and the nasofrontal suture, always above the line that connects the two inner canthi, identical to bony nasion
Otobasion inferius (Obi)	The most inferior point on the earlobe, located at the attachment (junction) of the lobe to the face
Pogonion (Pog)	The most anterior midpoint of the chin, located on the skin surface in front of the identical bony landmark of the mandible
Pronasale (Prn)	The most protruded point of the apex nasi identified in lateral view of the rest position of the head
Stomion inferius (Sti)†	The most superior midpoint of the vermilion border of the lower lip
Stomion superius (Sts)†	The most inferior midpoint of the vermilion border of the upper lip when the lips are at rest; with closed lips, this point will fall over Sti
Subnasale (Sn)	The midpoint of the angle at the columella base where the lower border of the nasal septum and surface of the upper lip meet; not identical to the bony point ANS or nasospinale
Subtragion (Sbtr)†	The most anterior inferior point on the anterior inferior margin of the helix attachment to the face, just above the earlobe
Superior labial sulcus (SLS)†	The deepest midline point on the upper lip, which is located usually halfway between Sn and Ls
Tragion (Tr)	The notch on the upper margin of the tragus
Zygion (Zyg)†	The most prominent point on the cheek area beneath the outer canthus and slightly medial the vertical line passing through it; different from bony zygion

*The authors preferred to use the first term instead of the second term chosed by Farkas.[38]
†Points defined by the authors.

Table 2 Mean x-, y-, and z-differences (in mm) of 30 landmarks on 3D models

Landmarks	Mean x-difference (SD)	Mean y-difference (SD)	Mean z-difference (SD)
AcL	0.16 (0.13)	0.36 (0.27)	0.37 (0.29)
AcR	0.12 (0.08)	0.43 (0.24)	0.41 (0.31)
ChL	0.35 (0.20)	0.22 (0.16)	0.21 (0.16)
ChR	0.36 (0.26)	0.24 (0.14)	0.17 (0.13)
EncL	0.48 (0.49)	0.24 (0.17)	0.14 (0.16)
EncR	0.32 (0.21)	0.24 (0.14)	0.14 (0.15)
ExcL	0.28 (0.21)	0.28 (0.26)	0.34 (0.33)
ExcR	0.19 (0.16)	0.30 (0.24)	0.33 (0.26)
Gl	0.50 (0.23)	0.70 (0.52)	0.14 (0.11)
GoL	1.18 (1.08)	2.89 (2.89)	2.00 (1.70)
GoR	1.06 (0.49)	2.36 (1.86)	2.97 (1.75)
ILS	0.34 (0.16)	0.46 (0.28)	0.12 (0.14)
Li	0.46 (0.19)	0.29 (0.16)	0.10 (0.07)
Ls	0.27 (0.12)	0.33 (0.42)	0.11 (0.10)
Me	0.70 (0.54)	0.40 (0.27)	1.07 (0.56)
N	0.35 (0.37)	0.42 (0.26)	0.08 (0.05)
ObiL	0.19 (0.13)	0.48 (0.33)	0.62 (0.31)
ObiR	0.32 (0.34)	0.48 (0.35)	0.88 (0.57)
Pog	0.43 (0.27)	0.40 (0.36)	0.06 (0.03)
Prn	0.31 (0.20)	0.39 (0.38)	0.06 (0.05)
SbtrL	0.07 (0.06)	0.34 (0.23)	0.49 (0.32)
SbtrR	0.08 (0.05)	0.29 (0.22)	0.48 (0.28)
SLS	0.27 (0.20)	0.45 (0.28)	0.05 (0.03)
Sn	0.13 (0.10)	0.29 (0.24)	0.23 (0.11)
Sti	0.34 (0.15)	0.29 (0.13)	0.18 (0.11)
Sts	0.22 (0.16)	0.20 (0.13)	0.42 (0.37)
TrL	0.15 (0.17)	1.12 (0.60)	1.24 (0.65)
TrR	0.32 (0.27)	1.12 (1.09)	1.32 (0.71)
ZygL	0.69 (0.65)	0.63 (0.76)	0.44 (0.36)
ZygR	0.66 (0.65)	0.80 (0.79)	0.58 (0.60)

several points showed poor reproducibility, including Go, Me, Zyg, and Tr (Fig 8).

Discussion

The reproducibility of Go and Zyg points was poor, due to the difficulty in locating these points precisely on the screen. Locating these would require palpation on the face and marking them prior to capture. Recognizing soft tissue Me was difficult, especially in patients with double chin and retrognathia.

The reproducibility of Tr was, surprisingly, lower than what had been expected (SD > 1.00 mm). The lack of brightness and contrast in the peripheral areas of the photorealistic-rendered model may have affected the accuracy in identifying that landmark. This problem may be overcome by adding a source of illumination on both sides when capturing the image. However, we found 2 additional points on each earlobe with reproducibility higher than tragion, ie, Sbtr and Obi (Table 2 and Fig 8). Sbtr was highly reproducible in the x-, y-, and z-axes, with a mean difference of 0.075 mm, 0.325 mm,

Table 3 Reproducibility of landmark identification on 3D models in the literature

Study	Type of analysis	No. of cases	Main results
McCance et al (1992) using laser scanning[3]	Differences in x, y, z coordinates of repeated digitization of 10 soft tissue landmarks	10 (5 control, 5 Class III patients)	The mean difference in repeated digitization was between 0.02 and 0.82 mm in the x-axis, 0.05 and 0.32 mm in the y-axis, and 0.01 and 0.59 mm in the z-axis
Moss et al (1994) using laser scanning[4]	Differences in x, y, z coordinates of 10 soft tissue landmarks	10 (5 control, 5 Class II patients)	The mean difference in repeated digitization was between 0.02 and 0.82 mm in the x-axis, 0.05 and 0.32 mm in the y-axis, and 0.01 and 0.59 mm in the z-axis
Ferrario et al (1997) using 3DFM technique[39]	Differences in repeated direct identification of 16 soft tissue landmarks (on patients' faces)	Not available	The overall error was 2 mm
Ras et al (1996) using a stereophotogrammetric system[27]	Differences between repeated 3D linear and angular measurements using 5 soft tissue points	10 children	The greatest difference was 1.0 mm for linear measurements and 1.1 degrees for angular measurements

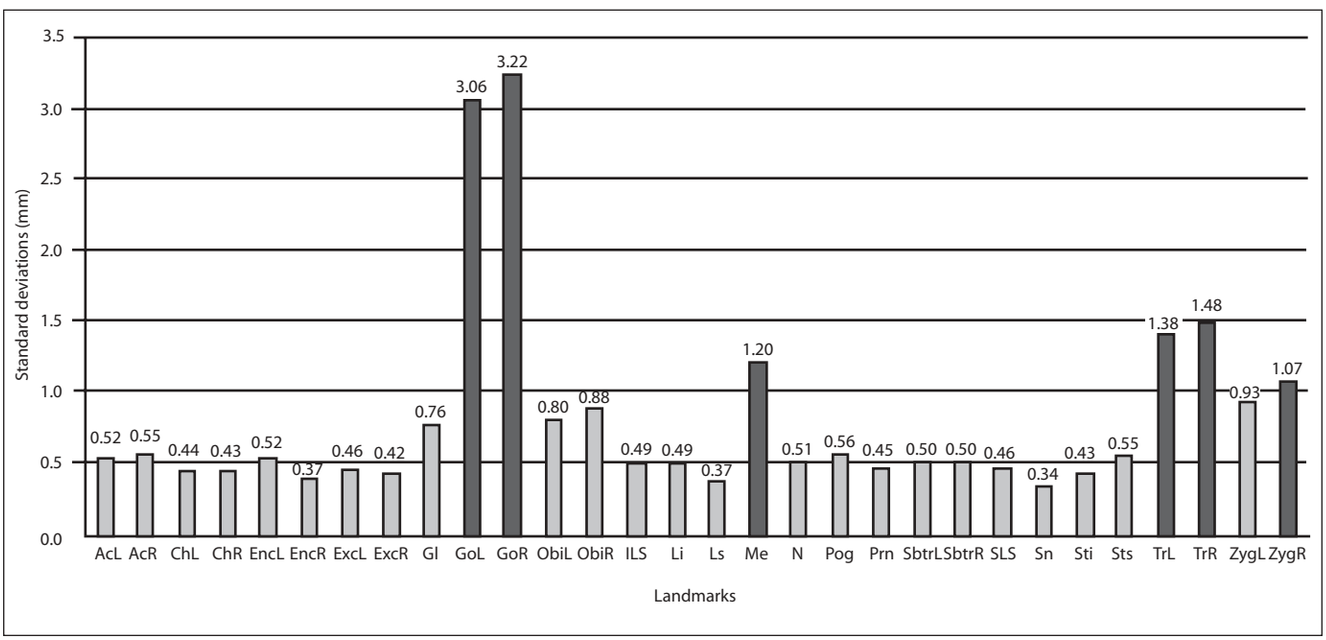

Fig 8 Reproducibility of landmark identification. Landmarks for which the standard deviations exceeded the 1-mm limit were considered inappropriate for use in studying facial soft tissue changes (columns marked in dark gray).

and 0.485 mm, respectively (right and left values of this point [Sbtr] in each axis were combined and averaged).

Using the centroid of a number of repeated placements has the advantage that its variability will be less than singularly placed landmarks. Specifically, the standard deviation of the averaged value will be inversely proportional to the square root of the number of values averaged, eg, the standard deviation of the average of 4-times-placed landmarks will be approximately half the standard deviation of a singularly placed landmark. This can be employed to improve reproducibility of "difficult" landmarks such as Me and Tr.

Table 3 illustrates the reproducibility of landmark identification conducted in other 3D studies. It appeared that our landmark identification reproducibility was higher than what was quoted by Ferrario et al,[39] who found an overall error of 2 mm. However, our reproducibility was slightly less than that obtained by Moss et al,[4] who performed their tests using 10 soft tissue landmarks identified on laser scans for averaging and superimpositioning purposes. We tried, in our investigation, to explore the reproducibility of 30 landmarks covering areas such as the cheeks, gonial angles, the chin, and the ear, which were not included in previous studies.[3–5,27] In the current investigation, landmark identification was done by one operator, and it would be interesting to study the variability in landmark identification between different operators working on the same 3D models.

For studying the displacement of soft tissue landmarks for consecutive orthognathic cases, models need to be registered in a 3D manner. Our plan of calculating the x, y, z displacements of soft tissue landmarks depends on the use of partial ordinary Procrustes analysis (partial because the analysis does not include scaling of the 3D coordinates). Based on the results of this investigation about landmark identification reproducibility, we were able to create a list of 7 points that should be used in superimposing 2 models per patient; namely, right and left Exc, right and left End, N, and right and left Sbtr. These points proved to be stable over time, ie, not affected by surgery, and highly reproducible. An example of a 3D superimposition of a Class II case corrected by bilateral inverted-L osteotomy is shown in Fig 9. Landmark-based soft tissue changes can be calculated after aligning 3D models on these 7 points, and the magnitude of surgical change, along with the possible postsurgical relapse, can be evaluated. This technique will be used in analyzing facial changes following orthognathic surgery in our ongoing study of Class II and Class III dentofacial deformities in the west of Scotland.

Fig 9 An example of two 3D models of a skeletal Class II patient pre- and postoperatively superimposed. Seven points were used for this registration.

Acknowledgments

We would like to thank Mr D. Koppel, Mr G. Wood, and Mr N. Hammersley, Consultants in Oral and Maxillofacial Surgery at Canniesburn and Monklands Hospitals, as well as Mr D. Whiteford for his technical support. We would also like to acknowledge the UK Department of Trade and Industry for funding the Imaging Faraday Partnership at Glasgow University.

References

1. Ayoub AF, Wray D, Moos KF, et al. Three-dimensional modeling for modern diagnosis and planning in maxillofacial surgery. Int J Adult Orthod Orthognath Surg 1996;11:225–233.
2. Rabey G. Craniofacial morphanalysis. Proc R Soc Med 1971;64:103–111.
3. McCance AM, Moss JP, Wright WR, Linney AD, James DR. A three-dimensional soft tissue analysis of 16 skeletal Class III patients following bimaxillary surgery. Br J Oral Maxillofac Surg 1992; 30:221–232.
4. Moss JP, McCance AM, Fright WR, Linney AD, James DR. A three-dimensional soft tissue analysis of fifteen patients with Class II, Division 1 malocclusions after bimaxillary surgery. Am J Orthod Dentofacial Orthop 1994;105:430–437.
5. McCance AM, Moss JP, Fright WR, James DR, Linney AD. A three dimensional analysis of soft and hard tissue changes following bimaxillary orthognathic surgery in skeletal III patients. Br J Oral Maxillofac Surg 1992;30:305–312.
6. Bill JS, Reuther JF, Dittmann W, et al. Stereolithography in oral and maxillofacial operation planning. Int J Oral Maxillofac Surg 1995;24:98–103.
7. Hell B. 3D sonography. Int J Oral Maxillofac Surg 1995;24:84–89.

8. Ferrario VF, Sforza C, Serrao G, Puletto S, Bignotto M, Tartaglia G. Comparison of soft tissue facial morphometry in children with Class I and Class II occlusions 72. Int J Adult Orthod Orthognath Surg 1994;9:187–194.
9. Ferrario VF, Sforza C, Poggio CE, Serrao G, Miani A Jr. A three-dimensional study of sexual dimorphism in the human face. Int J Adult Orthod Orthognath Surg 1994;9:303–310.
10. Nanda RS, Ghosh J, Bazakidou E. Three-dimensional facial analysis using a video imaging system. Angle Orthod 1996;66:181–188.
11. Kawai T, Natsume N, Shibata H, Yamamoto T. Three-dimensional analysis of facial morphology using moire stripes. Part I. Method. Int J Oral Maxillofac Surg 1990;19:356–358.
12. Leivesley WD. The reliability of contour photography for facial measurements. Br J Orthod 1983;10:34–37.
13. Savara BS. A method for measuring facial bone growth in three dimensions. Hum Biol 1965;37: 245–255.
14. Baumrind S, Moffitt FH, Curry S. The geometry of three-dimensional measurement from paired coplanar x-ray images. Am J Orthod 1983;84: 313–322.
15. Grayson B, Cutting C, Bookstein FL, Kim H, McCarthy JG. The three-dimensional cephalogram: Theory, technique, and clinical application. Am J Orthod Dentofacial Orthop 1988;94:327–337.
16. Xia J, Wang D, Samman N, Yeung RW, Tideman H. Computer-assisted threedimensional surgical planning and simulation: 3D color facial model generation. Int J Oral Maxillofac Surg 2000;29: 2–10.
17. Xia J, Ip HH, Samman N, et al. Computer-assisted three-dimensional surgical planning and simulation: 3D virtual osteotomy. Int J Oral Maxillofac Surg 2000;29:11–17.
18. Motoyoshi M, Namura S, Arai HY. A three-dimensional measuring system for the human face using three-directional photography. Am J Orthod Dentofacial Orthop 1992;101:431–440.
19. Ferrario VF, Sforza C, Schmitz JH, Santoro F. Three-dimensional facial morphometric assessment of soft tissue changes after orthognathic surgery. Oral Surg Oral Med Oral Pathol Oral Radiol Endod 1999;88:549–556.
20. Thompson MM (ed). Manual of Photogrammetry, ed 3. Falls Church, VA: American Society of Photogrammetry, 1966.
21. Burke PH, Beard FH. Stereophotogrammetry of the face. A preliminary investigation into the accuracy of a simplified system evolved for contour mapping by photography. Am J Orthod 1967; 53:769–782.
22. Beard LF, Burke PH. Evolution of a system of stereophotogrammetry for the study of facial morphology. Med Biol Illus 1967;17:20–25.
23. MacGregor AR, Newton I, Gilder RS. A stereophotogrammetric method of investigating facial changes following the loss of teeth. Med Biol Illus 1971;21:75–82.
24. Bjorn H, Lundquist C, Hjelstrom P. A photogrammetric method of measuring the volume of facial swellings. J Dent Res 1954;33:295–308.
25. Berkowitz S, Cuzzi J. Biostereometric analysis of surgically corrected abnormal faces. Am J Orthod 1977;72:526–538.
26. Kobayashi T, Ueda K, Honma K, Sasakura H, Hanada K, Nakajima T. Threedimensional analysis of facial morphology before and after orthognathic surgery. J Craniomaxillofac Surg 1990;18: 68–73.
27. Ras F, Habets LL, van Ginkel FC, Prahl-Andersen B. Quantification of facial morphology using stereophotogrammetry—Demonstration of a new concept. J Dent 1996;24:369–374.
28. Techalertpaisarn P, Kuroda T. Three-dimensional computer-graphic demonstration of facial soft tissue changes in mandibular prognathic patients after mandibular sagittal ramus osteotomy. Int J Adult Orthod Orthognath Surg 1998;13:217–225.
29. Nguyen CX, Nissanov J, Ozturk C, Nuveen MJ, Tuncay OC. Three-dimensional imaging of the craniofacial complex. Clin Orthod Res 2000; 3:46–50.
30. McDonald JP, Siebert JP, Fryer RJ, Urquhart CW. Visualization and model building in medical imaging. Med Inform 1993;19:61–69.
31. Mowforth PH, Ayoub AF, Jin J, et al. 3D imaging system for clinical applications. Med Electronics 1995;26:59–63.
32. Zhengping J. On the Multi-Scale Iconic Representation for Low-Level Computer Vision Systems [thesis]. Glasgow: The Turing Institute and The University of Strathclyde, 1988.
33. Ayoub AF, Siebert P, Moos KF, Wray D, Urquhart C, Niblett TB. A vision-based three-dimensional capture system for maxillofacial assessment and surgical planning. Br J Oral Maxillofac Surg 1998; 36:353–357.
34. Siebert JP, Marshall SJ. Human body 3D imaging by speckle texture projection photogrammetry. Sensor Rev 2000;20:218–226.
35. Ayoub A, Garrahy A, Hood C, et al. Validity of a new method of assessment of facial deformities in three dimensions. Cleft Palate Craniofac J [in press].
36. Lorensen WE, Cline HE. Marching cubes: A high-resolution 3D surface construction algorithm. Comput Graph 1987;21:163–169.
37. Mao Z, Siebert JP, Ayoub AF. Development of 3D measuring techniques for the analysis of facial soft tissue change. Proc Medical Image Computing and Computer-Assisted Intervention 2000 (MICCAI 2000), Pittsburgh, USA, 2000.
38. Farkas LG. Examination. In: Farkas LG (ed). Anthropometry of the Head and Face, ed 2. New York: Raven Press, 1994:20–26.
39. Ferrario VF, Sforza C, Poggio CE, Colombo A, Tartaglia G. The relationship between facial 3-D morphometry and the perception of attractiveness in children. Int J Adult Orthod Orthognath Surg 1997;12:145–152.